UNIVERSITY
OF OSLO

Master's thesis

-sometitle-

Classifying N-body simulations with and without relativistic corrections
using machine learning techniques

Johan Mylius Kroken

Computational Science: Astrophysics
60 ECTS study points

Institute of Theoretical Astrophysics
Faculty of Mathematics and Natural Sciences

Autumn 2023

Johan Mylius Kroken

-sometitle-

Classifying N-body simulations with and without relativistic corrections using machine learning techniques

Supervisors:
A David Fonseca Mota
B Julian Adamek
C Francisco Antonio Villaescusa Navarro

Abstract

On large scales, comparable to the horizon, relativistic effects will affect the cosmological observables. In order to solve for these effects, one need to consistently solve for the metric, velocities and densities in a particular gauge. When simulating large-scale structures we use N-body simulations, which are usually performed in the Newtonian limit. However, it is not obvious that Newtonian gravity yield a good global description of an inhomogeneous cosmology across all scales (Jeong, Fabian Schmidt and Hirata 2012). However, literature suggest that Newtonian simulations are still solving the dynamics correctly, even on large scales close to the horizon where relativistic effects are important but may be corrected for (Chisari and Zaldarriaga 2011) (Green and Wald 2012).

Recently, Adamek et al. 2016 developed a relativistic N-body code, `gevolution`, which evolves large scales structures based on the weak field expansion in GR. I investigate the differences in the gravitational dynamics between structures evolved with and without relativistic effects, with focus on the gravitational potential Φ. This is a good choice for comparison as Φ is gauge invariant and the Newtonian and relativistic simulations are performed in different gauges.

The investigation is done by running 2000 simulations using identical ΛCDM cosmologies for the two gravity theories. The simulations are run using 64^4 particles on a 256^3 grid each with dimension 5120 Mpc/h which is a compromise in order to include both large and nonlinear scales. The data analysis consist of a preliminary analysis using conventional summary statistics, with focus on the bispectrum of Φ. There is a difference in the two cases for low redshifts in the equilateral and squeezed configurations. However, the main idea is to train a Convolutional Neural Network (CNN) to classify the two cases, given snapshots of Φ. The main analysis then involves interpretability of the CNN, which may be done by considering for instance saliency maps (Alqaraawi et al. 2020) or Grad-CAM (Selvaraju et al. 2020). In either case, revealing the features separating the two cases may help us understand the differences in the gravitational dynamics between the two theories. I expect that such a network is able to find relativistic corrections to the Newtonian snapshots that are of higher order than those obtained from power spectra and bispectra analysis. Further, it may also reveal which configurations of Fourier modes $\mathbf{k}$ yield the highest bispectral power, which for now is mainly trial and error.

Contents

List of Figures

List of Tables

Preface

Here comes your preface, including acknowledgments and thanks.

Part I

Cosmological Structure Formation

Chapter 2

Preliminaries

2.1 General Relativity

2.1.1 Einstein's Field Equations

$$G_{\mu\nu} = 8\pi G T_{\mu\nu} \tag{2.1}$$

$$G_{\mu\nu} = R_{\mu\nu} - \frac{1}{2} g_{\mu\nu} R \tag{2.2}$$

$$R = g^{\mu\nu} R_{\mu\nu} \tag{2.3}$$

$$R_{\mu\nu} = \partial_\rho \Gamma^\rho_{\mu\nu} - \partial_\nu \Gamma^\rho_{\mu\rho} + \Gamma^\rho_{\mu\nu} \Gamma^\sigma_{\rho\sigma} - \Gamma^\rho_{\mu\sigma} \Gamma^\sigma_{\nu\rho} \tag{2.4}$$

2.1.2 Riemann Connection and Covariant Derivatives

$$\Gamma^\rho_{\mu\nu} = \frac{1}{2} g^{\rho\sigma} \left(\partial_\mu g_{\nu\sigma} + \partial_\nu g_{\mu\sigma} - \partial_\sigma g_{\mu\nu} \right) \tag{2.5}$$

$$\nabla_\mu T^\mu_\nu = \partial_\mu T^\mu_\nu + \Gamma^\mu_{\mu\alpha} T^\alpha_\nu - \Gamma^\alpha_{\mu\nu} T^\mu_\alpha \tag{2.6}$$

2.1.3 Geodesic Equation

$$\frac{d^2 x^\mu}{d\tau^2} + \Gamma^\mu_{\alpha\beta} \frac{dx^\alpha}{d\tau} \frac{dx^\beta}{d\tau} = 0 \tag{2.7}$$

2.1.4 The Stress-Energy Tensor

$$T_{\mu\nu} = (\rho + p) u_\mu u_\nu + p g_{\mu\nu} \tag{2.8}$$

2.2 Useful Relations

Chapter 3

Background Cosmology

3.1 The homogeneous Universe

In this chapter I will focus on explaining the background cosmology in light of a homogeneous universe. A natural place to start is the cosmological principle, followed by a description of the geometry of space itself. If not otherwise stated, the development of this chapter is based on Dodelson and F. Schmidt 2020, Weinberg 2008 and TODO: cite Baumann

3.1.1 The Cosmological Principle

3.1.2 The Robertson-Walker Metric

$$ds^2 = -dt^2 + a^2(t)\left[\frac{dr^2}{1-kr^2} + r^2 d\Omega^2\right] \tag{3.1}$$

3.1.3 The Friedmann Equations

3.2 My Universe is loaded with...

3.3 Thermal History of the Universe

Chapter 4

Perturbation Theory

4.1 Initial Conditions

4.2 Transfer Functions

4.3 Power Spectra

4.4 Linear Evolution

4.5 Non-linear Evolution

4.6 Bispectra

The bispectra are powerful tools for studying the non-linear evolution of the density field. The bispectrum is defined as the Fourier transform of the three-point correlation function, and is given by:

$$\langle \delta(\mathbf{k}_1)\delta(\mathbf{k}_2)\delta(\mathbf{k}_3)\rangle = (2\pi)^3\delta_D\left(\sum_i \mathbf{k}_i\right) B(\mathbf{k}_1,\mathbf{k}_2,\mathbf{k}_3) \tag{4.1}$$

4.6.1 Analytical Bispectum

$$B_\delta^{(3)}(\mathbf{k}_1,\mathbf{k}_2,\mathbf{k}_3) = 2\mathcal{P}_\delta(k_1)\mathcal{P}_\delta(k_2)F_2(\mathbf{k}_1,\mathbf{k}_2) + \text{cyc} = 2\epsilon_{ijk}F_2(\mathbf{k}_j,\mathbf{k}_k)\mathcal{P}_\delta(k_j)\mathcal{P}_\delta(k_k) \tag{4.2}$$

$$F_2(\mathbf{k}_1,\mathbf{k}_2) = \frac{5}{7} + \frac{x}{2}\left(\frac{k_1}{k_2}+\frac{k_2}{k_1}\right) + \frac{2}{7}x^2, \tag{4.3}$$

where $x = \hat{\mathbf{k}}_1\cdot\hat{\mathbf{k}}_2 = \cos\theta_{12}$, where θ_{12} is the angle spanned by $\mathbf{k}_1$ and $\mathbf{k}_2$. We could thus consequently write: $F_2(\mathbf{k}_1,\mathbf{k_2}) = F_2(k_1,k_2,\theta_{12})$.

Work with kernel Given k_1 and k_2 and θ_{12} we have the following relations, with reference to Fig. 4.1:

$$\begin{aligned}\alpha &= \pi - \theta_{12}\\ \beta &= \pi - \theta_{23}\\ \gamma &= \pi - \theta_{31}\end{aligned} \tag{4.4}$$

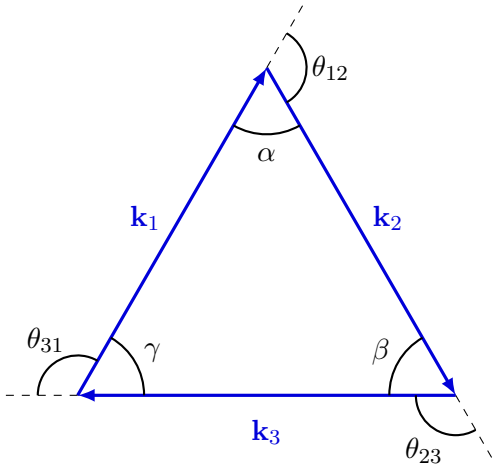

Figure 4.1: Angles in arbitrary bispectrum triangle configuration where $\sum_i \mathbf{k}_i = 0$.

From cosine rule:

$$k_3 = \sqrt{k_1^2 + k_2^2 - 2k_1 k_2 \cos\alpha} \tag{4.5}$$

From the rule of sines TODO: explain more?:

$$\begin{aligned} \beta &= \arcsin\left(\frac{k_1}{k_3}\sin\alpha\right) \\ \gamma &= \arcsin\left(\frac{k_2}{k_3}\sin\alpha\right) \end{aligned} \tag{4.6}$$

Bispectrum of potential Turn this into the bispectrum of the potential, and then use the Poisson equation to get the bispectrum of the density field. Start with the Poisson equation (at late times), valid for all scales as long as δ_m is given in synchronous gauge:

$$\begin{aligned} k^2\Phi(\mathbf{k},a) &= 4\pi G a^2 \rho_\mathrm{m}(a)\delta_\mathrm{m}(\mathbf{k},a) \\ \Phi(\mathbf{k},a) &= \frac{3}{2}\Omega_\mathrm{m}H_0^2\frac{\delta_\mathrm{m}(\mathbf{k},a)}{ak^2} = \mathcal{C}(k,a)\delta_\mathrm{m}(\mathbf{k},a) \end{aligned} \tag{4.7}$$

where in the last step I used that $\rho_\mathrm{m}(a) = \Omega_\mathrm{m}\rho_\mathrm{crit}a^{-3}$ and $8\pi G\rho_\mathrm{crit} = 3H_0^2$. I also defined the factor $\mathcal{C}(k,a)$ as follows:

$$\mathcal{C}(k,a) \equiv \frac{3\Omega_\mathrm{m}}{2a}\left(\frac{H_0}{k}\right)^2, \tag{4.8}$$

where $H_0/k = 1/(2997.13\cdot k)$ when k is given in units of h/Mpc. TODO: explain this more? This ensures that $\mathcal{C}(k,a)$ is dimensionless. The bispectrum of the potential is then given by:

$$\begin{aligned} \langle\prod_{i=1}^{3}\Phi(\mathbf{k}_i,a)\rangle &= \langle\prod_{i=1}^{3}\mathcal{C}(k_i,a)\delta_\mathrm{m}(\mathbf{k}_i,a)\rangle \\ B_\Phi(\mathbf{k}_1,\mathbf{k}_2,\mathbf{k}_3,a) &= B_\delta(\mathbf{k}_1,\mathbf{k}_2,\mathbf{k}_3,a)\prod_{i=1}^{3}\mathcal{C}(k_i,a). \end{aligned} \tag{4.9}$$

Using the same logic I find a relation between the power spectrum of the gravitational potential and the matter contrast:

$$\mathcal{P}_\Phi(k,a) = \mathcal{C}^2(k,a)\mathcal{P}_\delta(k,a) \Longleftrightarrow \mathcal{P}_\delta(k,a) = \mathcal{C}^{-2}(k,a)\mathcal{P}_\Phi(k,a) \tag{4.10}$$

which results in the following analytical bispectrum for the gravitational potential:[1]

$$B_\Phi^{(3)}(\mathbf{k}_1,\mathbf{k}_2,\mathbf{k}_3,a) = \prod_{n=1}^{3}\mathcal{C}(k_n,a)\left[\epsilon_{ijk}F_2(\mathbf{k}_j,\mathbf{k}_k)\prod_{l\in\{j,k\}}\mathcal{C}^{-2}(k_l,a)\mathcal{P}_\Phi(k_l,a)\right] \tag{4.11}$$

[1] Still only valid for even permutations of the Levi-Civita symbol of course.

Chapter 5

Simulation theory

Some theory and history as to how to conduct N-body simulations.

5.1 N-body simulations

5.1.1 Describing a box of particles

5.1.2 Forces and Fields

5.1.3 Mass Assignment Schemes

5.1.4 Validity of Box

5.2 Newtonian Approach

5.3 General Relativistic Approach

Part III

Acquiring Data

Chapter 9

Simulations

9.1 Parameters

When performing simulations, it was import to keep all parameters fixed for all the different simulations. The only thing that was changed was the random seed.

9.1.1 Cosmological parameters

The relevant cosmological parameters are the dimensionless Hubble factor h, the baryon and cold dark matter densities Ω_b and Ω_{CDM}, the Cosmic Microwave Background temperature T_{CMB} and the effective number of ultra-relativistic neutrinos N_{ur}.

Table 9.1: Cosmological parameters

Parameter	Value	Unit
h	0.67556	-
Ω_b	0.022032	-
Ω_{CDM}	0.12038	-
T_{CMB}	2.7255	K
N_{ur}	3.046	-

9.1.2 Primordial power spectrum

The primordial power spectrum, as TODO: link to when written,contains the pivot scale k_{piv}, the primordial amplitude, $\mathcal{A}_{\mathrm{s}}$ and the spectral index, n_{s}.

Table 9.2: Primordial power spectra parameters

Parameter	Value	Unit
k_{piv}	0.05	Mpc^{-1}
$\mathcal{A}_{\mathrm{s}}$	$2.215 \cdot 10^{-9}$	-
n_{s}	0.9619	-

9.1.3 Box parameters

The relevant box parameters were the initial redshift z_{ini} where the simulations were started from. The simulations box itself was characterised by the physical length L, represented on a cube grid of size N^3_{grid}, resulting in a resolution of $\Delta_{\text{res}} = L/N_{\text{grid}}$. The courant factor TODO: fill and time step limit TODO: fill. This resulted in a fundamental

Table 9.3: Box parameters

Parameter	Value	Unit
z_{ini}	100	
L	5120	Mpc
N_{grid}	256	px
Δ_{res}	$20 (= L/N_{\text{grid}})$	Mpc px^{-1}
Courant factor	48	?
Time step limit	0.04	?

frequency of $k_{\text{F}} = 2\pi/L$ and Nyquist freguency $k_{\text{N}} = \pi/\Delta_{\text{res}}$ TODO: what with units?

9.1.4 Seeds and gravity theories

One simulation consisted of two runs, one for each gravity theory, $\mathtt{T}$:

$$\mathtt{T} = \{\text{Newton}, \text{GR}\} \tag{9.1}$$

In order to initialise the simulations we used random seeds, one for each simulation. This ensured that analysis performed on different simulations were of different realisations of the simulated universe, essential statistical independence. The seeds, denoted as $\mathtt{S}$ ranged from 0 to 2000, and consisted of the following set:

$$\{\mathtt{S} \in \mathbb{Z} | 0 \leq \mathtt{S} < 2000\} \tag{9.2}$$

9.2 Output

9.2.1 Datacubes

The output of interest was the density field of the gravitational potential, Φ. This field was outputted at the following redshifts:

$$z_{\text{d}} = \{20, 15, 10, 5, 1, 0\} \tag{9.3}$$

One datacube was outputted for each redshift, for each seed, for each gravity theory and denoted $\mathcal{D}_{tzs}$, where $t \in \mathtt{T}$ is the gravity theory, $z \in z_{\text{d}}$ is the redshift and $s \in \mathtt{S}$ is the seed. This resulted in a total of $N_{\mathcal{D}} = N_{\mathtt{S}} N_{z_{\text{d}}} N_{\mathtt{T}} = 24000$ datacubes, each of size N^3_{grid}. Each dimension of the datacube can be indexed such that $i, j, k \in [1, N_{\text{grid}}]$. In this manner, one single data point corresponds to $\mathcal{D}^{ijk}_{tzs}$.

9.2.2 Redshift problem

There is however one issue with the redshift, the datacubes produced with the same seed for the same theory, but at different redshifts are highly dependent on each other. This is because they are the same realisations of the universe evolved with the same gravity theory, just evaluated at different times. In order to have a fully independent set of datacube, I consider only one redshift at a time, and denote the set of datacubes for a given redshift as $\mathcal{D}_z^{\text{ind}}$. This set consists of $N_{\mathcal{D}}^{\text{ind}} = N_{\mathcal{D}}/N_{z_{\text{d}}} = 4000$ datacubes.

9.2.3 Statistics of dataset

The statistics of the dataset is evaluated for each independent dataset, i.e. for each redshift. The mean of one single datacube is therefore explicitly given by:

$$\bar{\mathcal{D}}_{tzs} = \frac{1}{N_{\text{grid}}^3} \sum_{i=1}^{N_{\text{grid}}} \sum_{j=1}^{N_{\text{grid}}} \sum_{k=1}^{N_{\text{grid}}} \mathcal{D}_{tzs}^{ijk}, \tag{9.4}$$

and the mean of the independent dataset is given by:

$$\mu_z = \frac{1}{N_{\mathcal{D}}^{\text{ind}}} \sum_{t \in \mathtt{T}} \sum_{s \in \mathtt{S}} \bar{\mathcal{D}}_{tzs}. \tag{9.5}$$

The variance of the independence dataset is thus given by:

$$\text{Var}_z = \frac{1}{N_{\mathcal{D}}^{\text{ind}} N_{\text{grid}}^3} \sum_{t \in \mathtt{T}} \sum_{s \in \mathtt{S}} \sum_i \sum_j \sum_k \left(\mathcal{D}_{tzs}^{ijk} - \mu_z \right)^2, \tag{9.6}$$

and the corresponding standard deviation:

$$\sigma_z = \sqrt{\text{Var}_z}. \tag{9.7}$$

Question: Include actual numerical values?
Question: Include some figure?

9.2.4 Normalisation

Each independent set of datacubes may then be normalised by subtracting the mean and dividing by the standard deviation. This ensures a zero mean and unit variance across the set, without loosing the monopole and dipole of the data. The normalised datacubes are denoted $\mathcal{D}_z^{\text{norm}}$ and are given by:

$$\mathcal{D}_z^{\text{norm}} = \frac{\mathcal{D}_z^{\text{ind}} - \mu_z}{\sigma_z}, \tag{9.8}$$

which will be the set(s) used for training and testing the machine learning algorithms.

Chapter 10

Data Verification

10.1 Slices of Datacubes

10.2 Powerspectra from Simulations

10.3 Powerspectra from Datacubes

10.4 Analytical Bispectra

10.5 Bispectra from Cube

10.5.1 Binning

10.5.2 Bispectra

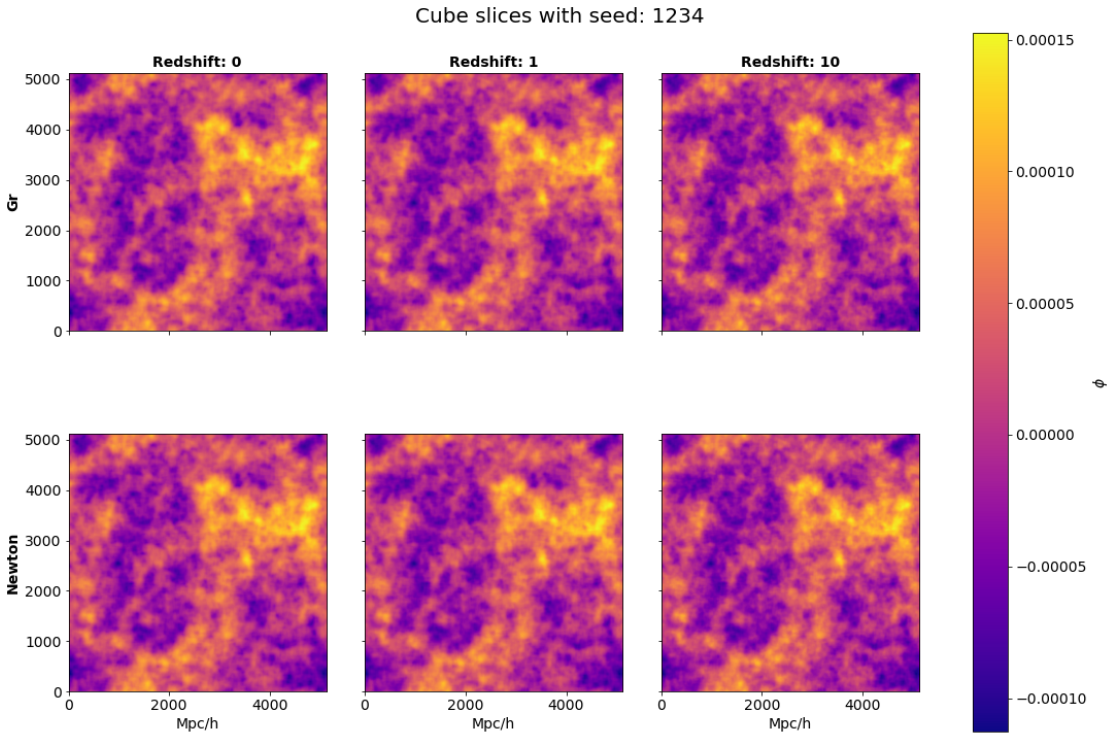

Figure 10.1: Slice 0

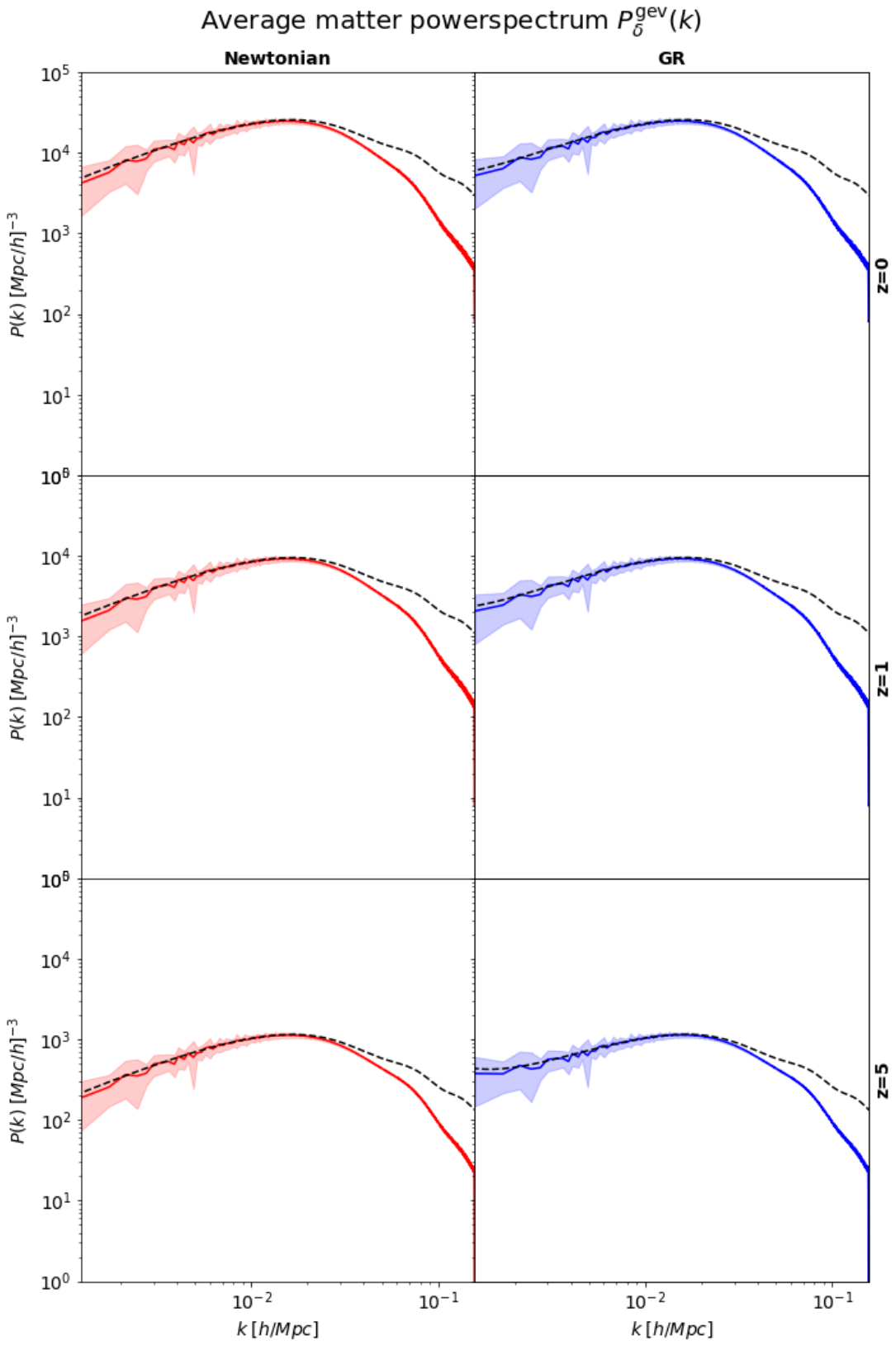

Figure 10.2: Average matter power spectra at different redshifts.

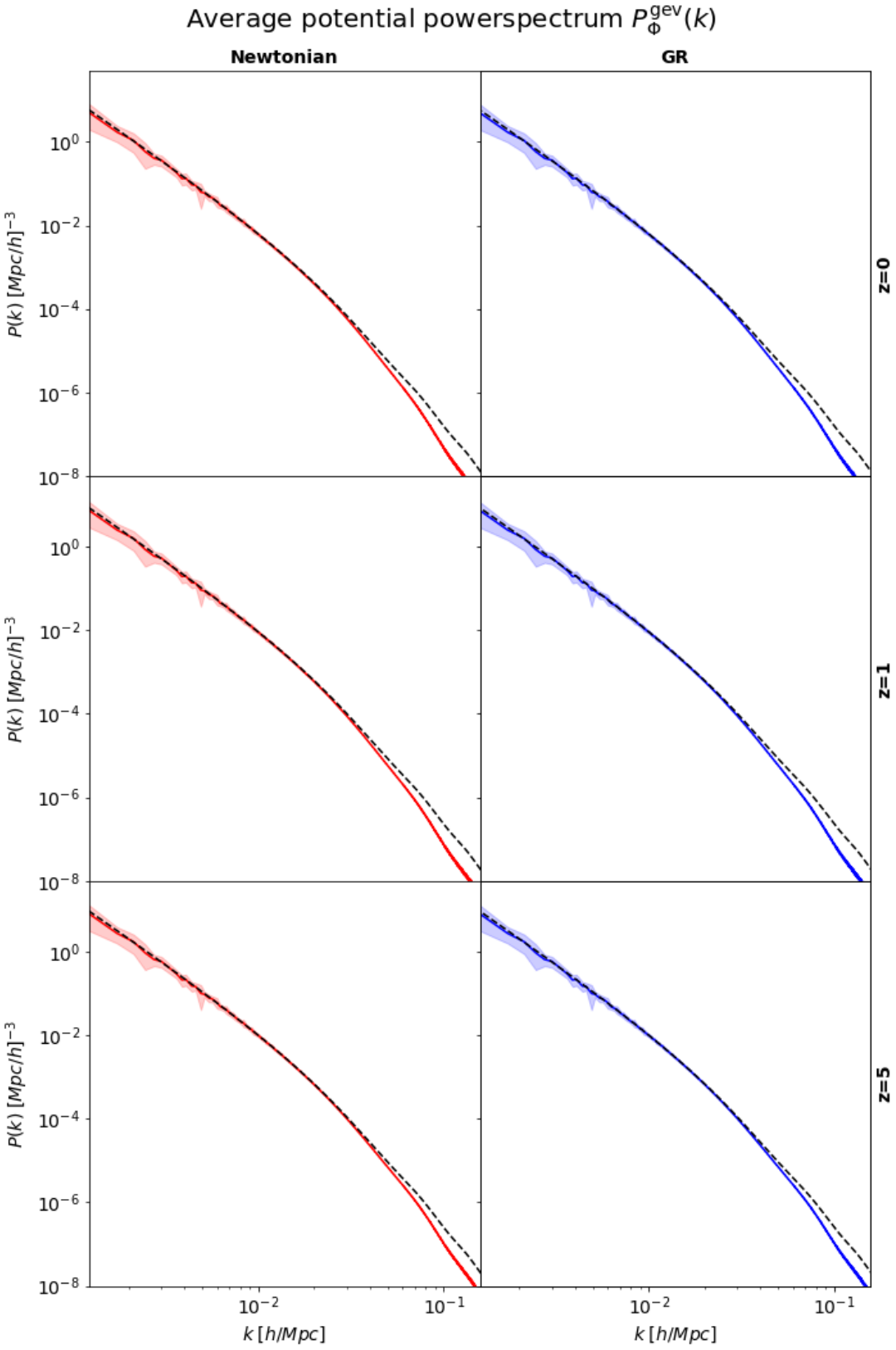

Figure 10.3: Average potential power spectra at different redshifts.

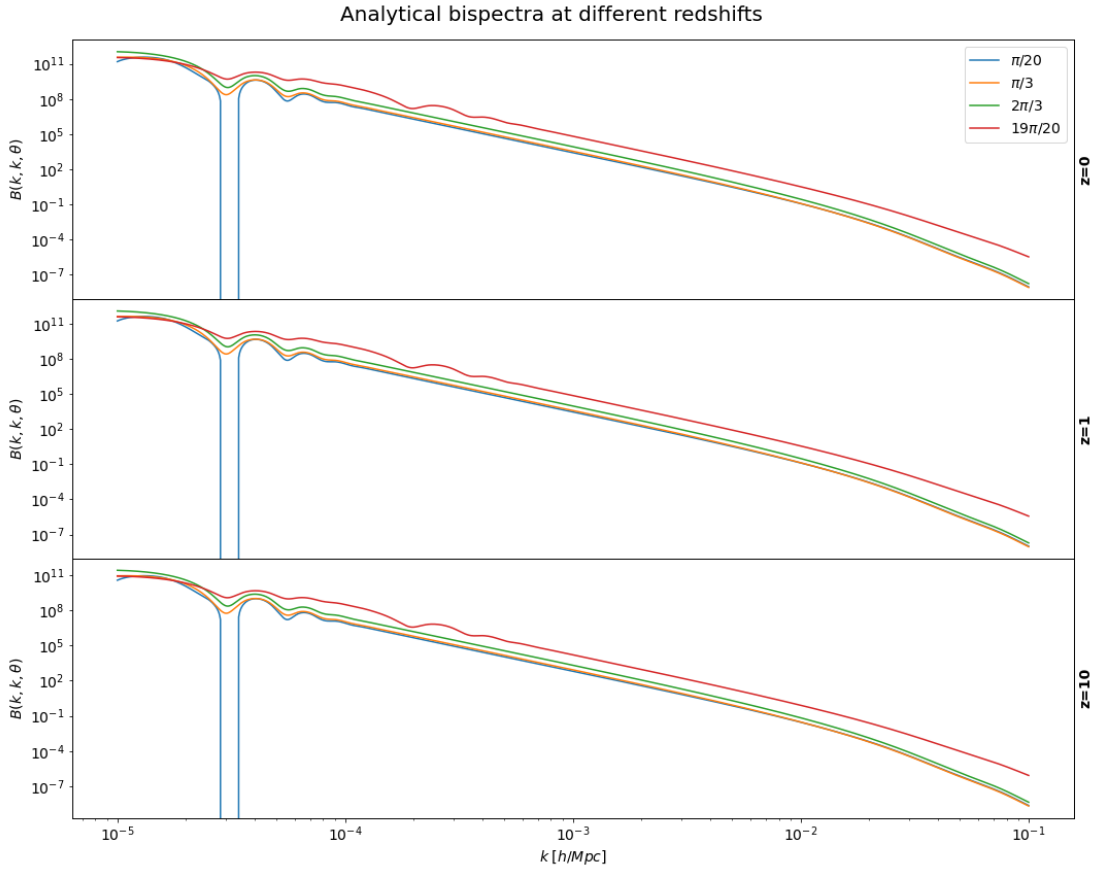
Analytical bispectra at different redshifts
π/20
π/3
2π/3
19π/20
B(k, k, θ)
z=0
z=1
z=10
k [h/Mpc]

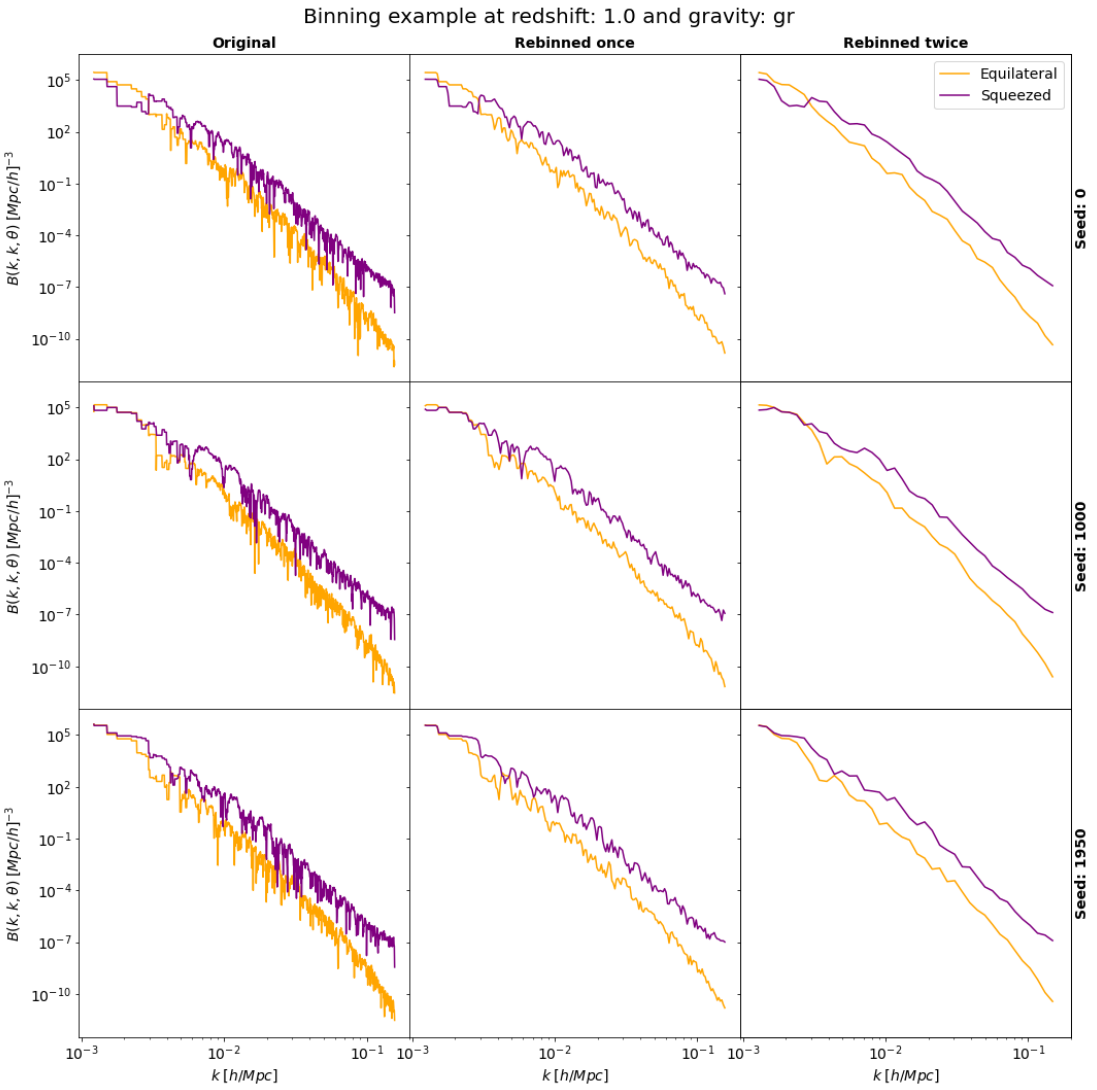
Binning example at redshift: 1.0 and gravity: gr
Original
Rebinned once
Rebinned twice
Equilateral
Squeezed
Seed: 0
Seed: 1000
Seed: 1950
$B(k,k,\theta)\ [Mpc/h]^{-3}$
$k\ [h/Mpc]$

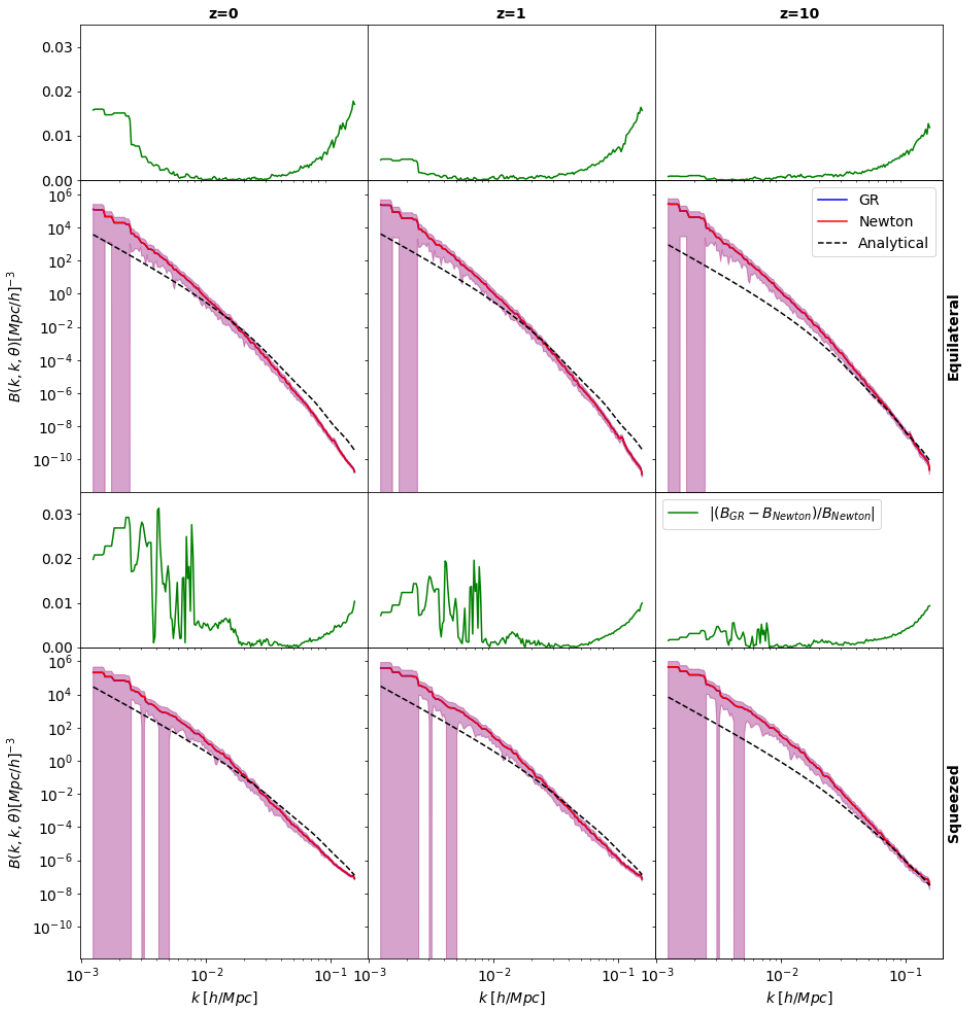
z=0
z=1
z=10
GR
Newton
Analytical
$|(B_{GR} - B_{Newton})/B_{Newton}|$
Equilateral
Squeezed
$B(k, k, \theta)[Mpc/h]^{-3}$
$k\,[h/Mpc]$

Chapter 11

Trainable Dataset

The raw data are the set of cubes generated for each random seed `S`, at each redshift z_d for both gravity theories. This need to be converted into a trainable dataset for use with a machine learning algorithm. One possibility is to pass the whole cube as input data into an algorithm. However, for algorithms like CNNs this is not a good idea as it would involve three-dimensional convolutional kernels which greatly increase the training time of the network TODO: source?. Instead, I will use a method similar to the one used by TODO: find source for this where they used a two-dimensional slice of the three-dimensional cube as input data. I will refer to one such slice as an *image*. Following this, I extract slices from each datacube, along all axes with a stride $\mathcal{S}$. This will result in a total of $\mathcal{I}_\mathrm{cube} = N_\mathrm{axes} N_\mathrm{grid}/\mathcal{S}$ images per cube, with dimensions $(\mathcal{S}, N_\mathrm{grid}, N_\mathrm{grid})$. The whole dataset will then consist of $\mathcal{I}_\mathrm{tot} = \mathcal{I}_\mathrm{cube} N_\mathrm{cube}$ images.

11.1 Gathering the cubes

Since the output from each redshift

11.2 Find image from index

Given an index i of an image in the dataset, I need to find the corresponding cube, redshift and slice. This is done by the following algorithm, where $i \in [0, \mathcal{I}_\mathrm{tot})$: The algorithm is explained in detail in Algorithm 1. In the first procedure I find the datacube from the index i, and in the second I find the index of the slice corresponding to the desired image for a given datacube. This logic is illustrated in Section 11.2, where I highlight two possible "paths" from an index to the desired image. For the red path, the datacube is a result of the Newtonian simulation and will be labeled accordingly. It also corresponds to some arbitrary redshift, but has seed 4. The desired image is the first second slice along the first axis. Comparable logic for the blue path, but this time the image comes from a GR simulation.

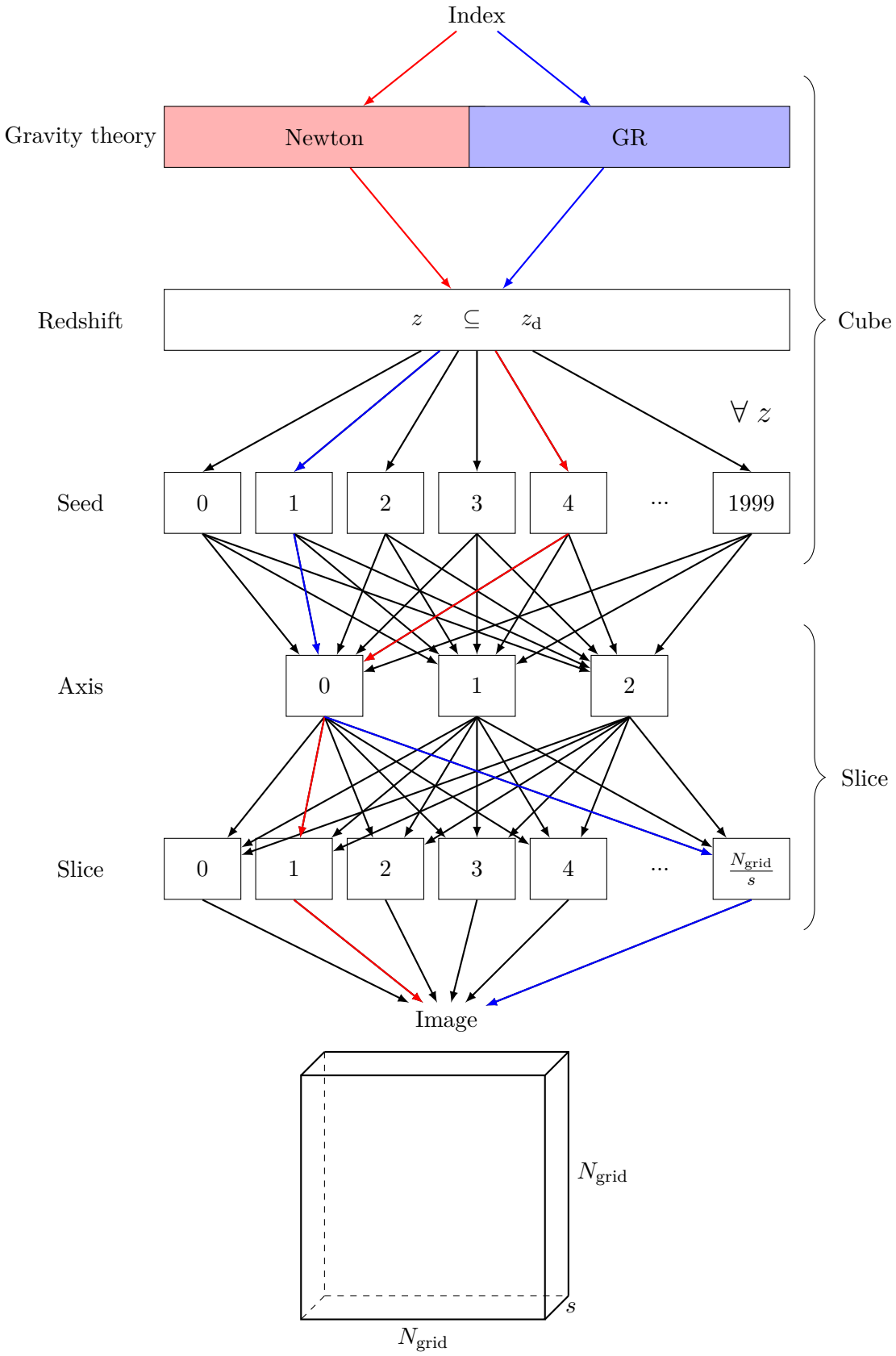

Figure 11.1: Outline of data structure.

Algorithm 1 Extract image from a given index i

procedure FINDCUBEFROMINDEX(i)
  $i_{\text{cube}} \leftarrow \left\lfloor \frac{i}{\mathcal{I}_{\text{cube}}} \right\rfloor$ ▷ Convert to one index per cube
  $i_{\text{gravity}} \leftarrow \left\lfloor \frac{i_{\text{cube}}}{N_z N_{\text{S}}} \right\rfloor$ ▷ Gravity index: 0 for Newton, 1 for GR
  $i_z \leftarrow \left\lfloor \frac{i_{\text{cube}}}{N_{\text{S}}} \right\rfloor \mod N_z$ ▷ Redshift index
  $i_{\text{S}} \leftarrow i_{\text{cube}} \mod N_{\text{S}}$ ▷ Index of seed
  return Cube$(i_{\text{gravity}}, i_z, i_{\text{S}})$ ▷ Array of shape $(N_{\text{grid}}, N_{\text{grid}}, N_{\text{grid}})$
end procedure
procedure FINDSLICEFROMCUBE(i)
  Cube $\leftarrow$ FINDCUBEFROMINDEX(i)
  $i_{\text{axis}} \leftarrow \left\lfloor \frac{i \mod \mathcal{I}_{\text{cube}}}{\mathcal{I}_{\text{cube}}/N_{\text{axis}}} \right\rfloor$ ▷ Index of axis
  $i_{\text{slice}} \leftarrow (i \mod \mathcal{I}_{\text{cube}}) \mod (\mathcal{I}_{\text{cube}}/N_{\text{axis}})$ ▷ Index of slice along given axis
  return Cube$[i_{\text{axis}}, i_{\text{slice}}]$ ▷ Array of size $(\mathcal{S}, N_{\text{grid}}, N_{\text{grid}})$
end procedure

Bibliography

Adamek, Julian et al. (29th July 2016). 'gevolution: a cosmological N-body code based on General Relativity'. In: *Journal of Cosmology and Astroparticle Physics* 2016.7, pp. 053–053. ISSN: 1475-7516. DOI: 10.1088/1475-7516/2016/07/053. arXiv: 1604.06065[astro-ph,physics:gr-qc,physics:physics]. URL: http://arxiv.org/abs/1604.06065 (visited on 23/08/2023).

Alqaraawi, Ahmed et al. (3rd Feb. 2020). *Evaluating Saliency Map Explanations for Convolutional Neural Networks: A User Study*. arXiv: 2002.00772[cs]. URL: http://arxiv.org/abs/2002.00772 (visited on 23/10/2023).

Chisari, Nora Elisa and Matias Zaldarriaga (2nd June 2011). 'Connection between Newtonian simulations and general relativity'. In: *Physical Review D* 83.12, p. 123505. ISSN: 1550-7998, 1550-2368. DOI: 10.1103/PhysRevD.83.123505. arXiv: 1101.3555[astro-ph,physics:gr-qc]. URL: http://arxiv.org/abs/1101.3555 (visited on 23/08/2023).

Dodelson, S. and F. Schmidt (2020). *Modern Cosmology*. Elsevier Science. ISBN: 9780128159484. URL: https://books.google.no/books?id=GGjfywEACAAJ.

Green, Stephen R. and Robert M. Wald (15th Mar. 2012). 'Newtonian and Relativistic Cosmologies'. In: *Physical Review D* 85.6, p. 063512. ISSN: 1550-7998, 1550-2368. DOI: 10.1103/PhysRevD.85.063512. arXiv: 1111.2997[astro-ph,physics:gr-qc]. URL: http://arxiv.org/abs/1111.2997 (visited on 23/08/2023).

Jeong, Donghui, Fabian Schmidt and Christopher M. Hirata (4th Jan. 2012). 'Large-scale clustering of galaxies in general relativity'. In: *Physical Review D* 85.2, p. 023504. ISSN: 1550-7998, 1550-2368. DOI: 10.1103/PhysRevD.85.023504. arXiv: 1107.5427[astro-ph]. URL: http://arxiv.org/abs/1107.5427 (visited on 23/08/2023).

Selvaraju, Ramprasaath R. et al. (Feb. 2020). 'Grad-CAM: Visual Explanations from Deep Networks via Gradient-based Localization'. In: *International Journal of Computer Vision* 128.2, pp. 336–359. ISSN: 0920-5691, 1573-1405. DOI: 10.1007/s11263-019-01228-7. arXiv: 1610.02391[cs]. URL: http://arxiv.org/abs/1610.02391 (visited on 23/10/2023).

Weinberg, S. (2008). *Cosmology*. Cosmology. OUP Oxford. ISBN: 9780191523601. URL: https://books.google.no/books?id=nqQZdg020fsC.